Inductive Heating Based on VHF-ISM Radio Band Frequencies as Technology Platform for Efficient Heating of Metallic Micro-Scaled Bonding Layers in MEMS Packaging

Christian Hofmann[1], Martin Kroll[2], Sushant Panhale[2], Maik Wiemer[1], Andreas Kunke[2], Karla Hiller[3], and Harald Kuhn[1,3]

[1]Fraunhofer Institute for Electronic Nano Systems ENAS, 09126 Chemnitz, Germany
[2]Institute for Machine Tools and Production Processes, University of Technology, 09126 Chemnitz, Germany
[3]Center for Microtechnologies, University of Technology, 09126 Chemnitz, Germany

This article presents a technique for selective and energy-efficient induction heating of aluminum (Al) frames to support and enhance the thermocompression bonding (TCB) for electronics packaging in the field of heterogeneous integration. The technological challenges include the use of an adapted induction coil for homogeneous heat distribution, the implementation of industrial, scientific, and medical (ISM) radio band frequencies in the high frequency (HF) and very high frequency (VHF) range up to $f_0 = 40.68$ MHz, and the assembly of a heating system based on an RF generator and automatic matching unit for impedance modulation. Finite element analysis (FEA) was used to calculate the electromagnetic (EM) fields based on the coil design used. The inductive heating was successfully carried out using a generator power of $P = 100$ W with coil currents in the range of $I_0 = 10.1$–11.3 A (amplitudes). With this setup, a peak temperature of $T_{f\_max} = 633$ °C in the Al frames could be achieved after $t_h = 10$ s. This corresponds to an average heating rate of $dT/dt = 63.3$ K/s.

***Index Terms*— Electromagnetic (EM) induction, electronics packaging, microelectromechanical systems (MEMS), radio frequency, selective heating.**

I. Introduction

HETEROGENEOUS integration is a key technology for assembling separate components into a higher system level [known as a system-in-package (SiP)] to enable enhanced functionality and improved operating characteristics [1]. As a result, bare dies, microelectromechanical systems (MEMS), passive components, and assembled packages are combined into a single package. To ensure high integration density with low failure rates, wafer and chip packaging processes have to meet complex industrial requirements. This involves the integration of components with widely varying coefficients of thermal expansion (CTE) and temperature-sensitive materials. In contrast, mechanically stable and hermetically sealed bond interfaces with high operating temperatures are required. In addition, industrial packaging processes using various thermal chip and wafer-level bonding techniques [e.g., eutectic bonding, soldering, thermocompression bonding (TCB), particle sintering] are significant cost drivers due to long process times and elevated energy consumption [2], [3]. These methods are based on global heating with process temperatures in the range of 250 °C–500 °C. As the thermal load is applied to the entire bond setup, the thermomechanical stress due to CTE mismatch has to be limited.

These temperature-related challenges can be addressed by selective and rapid heating technologies that apply energy locally to the desired area of the bond material itself. Beam-guided techniques are defined by a focused energy input but have economic and technical drawbacks, such as high setup costs, sequential processing, and accessibility [4]. Furthermore, integrated reactive material systems (iRMS) based on stacked material layers (e.g., Al/Pd, Al/Ti, Ti/Si) can be used as an internal energy source for selective heating [5]. However, the application of iRMS in heterogeneous integration is challenging due to complex manufacturing and material restrictions.

This article proposes an induction heating approach based on the high frequency (HF) and very high frequency (VHF) range with $f_0 = 13.56$–40.68 MHz. The technique allows the transfer of highly concentrated electromagnetic (EM) energy into electrically conductive materials with a high degree of efficiency [6]. Thus, micro-scale aluminum (Al) frames with great potential for MEMS packaging were investigated using finite element (FE) simulation and induction heating experiments. Previous work by the authors has been concerned with HF-based induction heating up to $f_0 = 2$ MHz for MEMS and power packaging [7], [8].

II. Theoretical Considerations

A. Heat Generation

In general, conductive heating is the dominant mechanism for introducing the thermal energy required for industrial packaging processes. The method is based on external currents and their ohmic resistance losses in a designated source component (e.g., hot plate). Thereby, heat propagates from the source to the load (here, the bond interface) primarily by thermal conduction, resulting in global heating of all components with a negative temperature gradient from the energy source to the interface. In contrast, inductive energy generation is based on the internal coupling of eddy currents with direct heating of the electrically conductive interface, resulting in a positive

Manuscript received 20 March 2023; revised 12 June 2023; accepted 12 June 2023. Date of publication 14 June 2023; date of current version 24 October 2023. Corresponding author: C. Hofmann (e-mail: christian.hofmann@enas.fraunhofer.de).

Color versions of one or more figures in this article are available at https://doi.org/10.1109/TMAG.2023.3286208.

Digital Object Identifier 10.1109/TMAG.2023.3286208

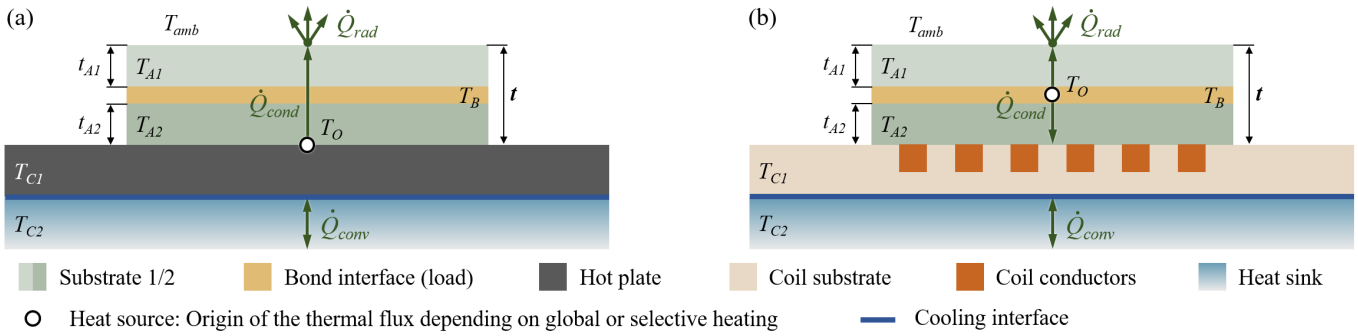

Fig. 1. Schematic of the heat transfer mechanisms: conduction, convection, and radiation. (a) Global temperature generation based on conductive heating using a hot plate. (b) Selective temperature generation based on inductive heating using an induction coil.

temperature gradient from the energy source (e.g., induction coil) to the bond interface. For further clarification, Fig. 1 illustrates both methods using the heat transfer mechanisms conduction $Q_{\text{cond\_Gl}}$ (1) related to global heating, conduction $Q_{\text{cond\_Se}}$ (2) related to selective heating, convection Q_{conv} (3), and radiation Q_{rad} (4). The different heat transfer modes can be described as

$$\dot{Q}_{\text{cond\_Gl}} = \frac{A_B \cdot \lambda}{t}\left(T_O - \left(\frac{T_{A1} + T_B + T_{A2}}{3}\right)\right) \tag{1}$$

$$\dot{Q}_{\text{cond\_Se}} = \frac{A_B \cdot \lambda}{t_{A1|A2}}\left(T_O - T_{A1|A2}\right) \tag{2}$$

$$\dot{Q}_{\text{conv}} = h \cdot A_C \cdot (T_{C1} - T_{C2}) \tag{3}$$

$$\dot{Q}_{\text{rad}} = \varepsilon \cdot \sigma \cdot A_{A1} \cdot \left(T_{A1}^4 - T_{\text{amb}}^4\right) \tag{4}$$

where T_{A1} and T_{A2} are the average temperatures of the substrates, T_B is the average temperature of the bond interface, T_{C1} is the average temperature of the hot plate and coil substrate, T_{C2} is the average temperature of the heat sink, T_O is the origin temperature of heat source, and T_{amb} is the average ambient temperature. In addition, λ is the thermal conductivity, h is the heat transfer coefficient, t_{A1} and t_{A2} are the thicknesses of the substrates, ε is the emissivity, and σ is the Stefan–Boltzmann constant. A_{A1} refers to the area of substrate 1, A_B to the area of the bond interface, and A_C to the area of the cooling interface.

B. Induction Heating

For induction heating, the Ampère–Maxwell law describes the generation of an EM field around a primary electrical conductor (induction coil) based on time-varying currents [6]. When the EM field passes through an electrically conductive material (the secondary conductor), a voltage is induced (Faraday's law of induction). The voltage causes a current in the opposite direction of coil current (Lenz's rule). According to Joule's law, the electrical energy E_{el} of the eddy currents I is converted into thermal energy Q_W (5), depending on the ohmic resistance R of the material and the time of energy supply t

$$Q_W = E_{\text{el}} = I^2 \cdot R \cdot t. \tag{5}$$

The amount of thermal energy transferred to the material depends on additional factors, such as the frequency f_0 of the primary EM field, the coil geometry, and the coupling distance between coil and material d. The higher the frequency, the more heat is concentrated on the material surface. This determines the skin depth δ, which can be expressed as follows:

$$\delta = \left(\sqrt{\pi \cdot f_0 \cdot \mu_r \cdot \mu_0 \cdot \kappa}\right)^{-1} \tag{6}$$

where μ_r is the relative permeability, μ_0 is the permeability of vacuum, and κ is the electrical conductivity of the secondary conductor. From the skin depth to the material surface, 86% of the electrical energy is converted to thermal energy [6].

TABLE I
GEOMETRIC PARAMETERS OF THE FRAMES

Symbol [a]	Parameter	Value
$\#_f$	frame quantity	4
-	frame material	Al (PVD)
h_f	frame thickness	2.0 µm
l_f	frame length	10.0 mm
w_f	frame width	10.0 mm
d_f	lateral frames distance [mm]	4
x_f	lateral frame width [µm]	500

[a]Symbolism according to Fig. 2.

III. DESIGN AND MODELING

A. Frame Design

The frame layout and materials were designed to be suitable for industrial Al-based TCB with the goal of hermetic MEMS encapsulation. The main parameters are listed in Table I. The frames were realized on silicon and glass (BOROFLOAT[1] 33) substrates using physical vapor deposition (PVD) of Al, photolithography, and wet chemical etching. The substrate size is 33 × 28 mm with a thickness of 675 μm for silicon and 500 μm for glass. Fig. 2 shows the substrates with the Al frames.

Al is a highly attractive material due to its low cost and compatibility with microelectronic processes. It can be directly integrated into established technologies (CMOS compatibility). However, due to the rapid surface formation of alumina (Al_2O_3) in the ambient atmosphere, solid-state TCB is very challenging and requires bond temperatures, pressures, and times of up to 500 °C, 100 MPa, and 2 h, respectively [9]. Based on the fusion welding of Al, the transition area from solid to liquid enables a fusion of the material [10]. This physical effect serves as a basis for future MEMS packaging using Al-based bonding and can be applied with the process characteristics of induction heating.

[1]Registered trademark.

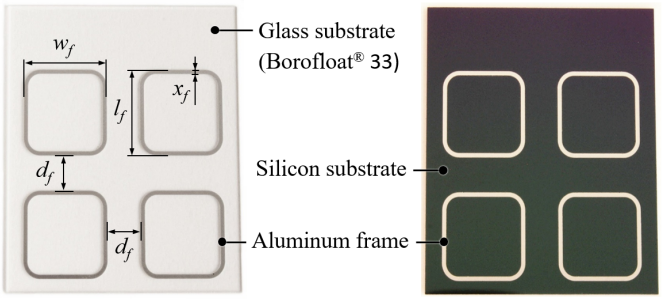

Fig. 2. Glass and silicon substrates with Al frames and main design parameters for FE simulation and induction heating experiments.

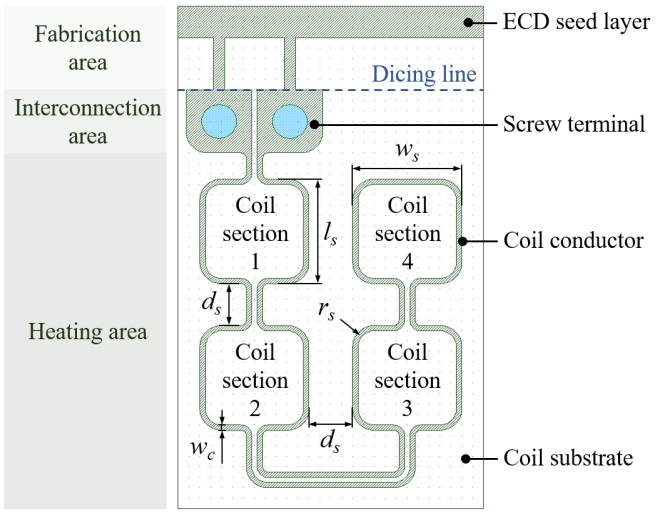

Fig. 3. Coil and conductor design with three main functional areas: fabrication, interconnection, and heating.

B. Coil Design

Fig. 3 shows the coil design based on a planar conductor geometry with a substrate size of 48 × 28 mm. The substrate thickness is 2 mm. The overall layout is divided into three functional areas to meet the different process demands of coil fabrication, electrical connection, and induction heating. The fabrication area contains an electrically conductive seed layer for electrochemical deposition (ECD) of the coil, which is linked to the interconnection area via two conductor paths. To interrupt the short circuit, the fabrication area is removed after coil completion. The interconnection area includes two pad geometries with through holes to provide a screw terminal for electrical connection to the induction generator. The heating area comprises the path of the coil conductor with four separate coil sections. Each section consists of a toroidal coil with outgoing and return lines. The coil circuit is electrically closed in Section IV. The conductor was made from copper using an ECD process. The coil was adapted to the frame layout and ensures homogeneous and rapid heating with a high efficiency. For a more detailed description of the coil conductor, the main geometric specifications are listed in Table II.

C. FE Simulation

In order to evaluate key performance parameters (e.g., frame temperature, heating rate, heat transfer) in the HF and VHF range of the EM spectrum, a frequency transient FE analysis

TABLE II
GEOMETRIC PARAMETERS OF THE COIL CONDUCTOR (HEATING AREA)

Symbol [a]	Parameter	Value
-	conductor material	Cu (ECD)
h_c	conductor thickness	0.5 mm
w_c	lateral conductor width	0.5 mm
$\#_s$	coil section quantity	4
l_s	section length	10.0 mm
w_s	section width	10.0 mm
r_s	section radius	1.75 mm
d_s	lateral section distance	4.0 mm
L	physical coil length (pads including)	209.8 mm

[a]Symbolism according to Fig. 3.

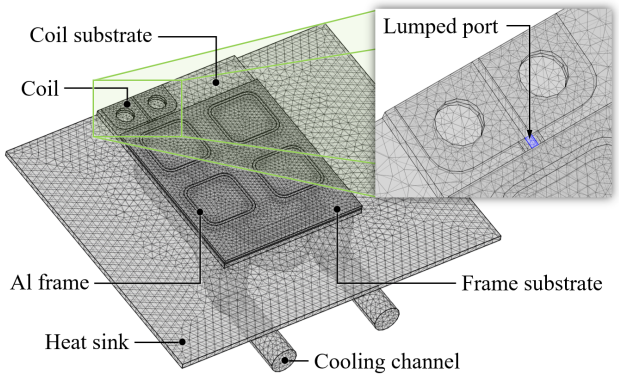

Fig. 4. Simulation model after meshing with main components and lumped port.

(FEA) was performed in COMSOL Multiphysics.[2] For this, the AC/DC module and the heat transfer module with the multiphysics coupled interfaces magnetic field, heat transfer in solids and fluids, laminar flow, and nonisothermal flow were used.

The geometric environment (Fig. 4) includes the definition of the main system components as domains (e.g., coil, frame, substrates), the specification of initial and boundary conditions (e.g., electrical and temperature-dependent parameters, virtual thickness), and the meshing of all components by using predefined tetrahedral elements calibrated to general physics. Material data (e.g., thermal conductivity, heat capacity) for the coil (copper), frames (Al), substrates (silicon and glass), and water channel were obtained from the COMSOL material database. The values for the coil substrate and heat sink (both aluminum nitride) were taken from the specific material data sheet. The coupling of the different physics interfaces is done by using variables and derived variables. Accordingly, each interface defines the equations, dependent variables, and a set of derived variables for the respective physics being simulated.

In addition to the typical physical challenges of absorption and reflection in induction heating, the EM spectrum in the HF and VHF range introduces the effect of standing waves caused by the electrical length G of the coil (7). This length, measured in wavelengths (8), is the distance traveled by an EM wave in one cycle at a specific frequency and can be calculated by

$$G = L/\lambda \tag{7}$$

$$\lambda = v_p/f_0 = c/f_0 \tag{8}$$

where L is the physical length of the coil, given in Table II for the coil design used, λ is the wavelength of the EM wave,

[2]Registered trademark.

TABLE III
ELECTRICAL LENGTH OF THE COIL DESIGN AS A FUNCTION OF FREQUENCY

Frequency f_0	Wavelength λ	Electrical length of the coil G
13.56 MHz	22.1 m	0.0094
27.12 MHz	11.1 m	0.0189
40.68 MHz	7.36 m	0.0285

v_p is the phase velocity (in the case of EM waves, the speed of light c), and f_0 is the frequency traveling through the coil.

If the wavelength is significantly larger than the physical length, the coil acts as a lumped circuit element. However, as the wavelength approaches the physical length of the coil, the electrical length gradually increases and the coil behaves as a distributed circuit element with varying impedance and admittance values along its length. This can lead to standing waves, so that the EM wave is unable to propagate through the coil without interaction or scattering, resulting in temperature peaks and valleys. The electrical length for the aforementioned coil design as a function of frequency is shown in Table III. The values indicate a very small electrical length close to zero with decreasing wavelength. Therefore, the influence of standing waves is very low with the coil design used. Nevertheless, the standing wave effect was considered in the FE model by implementing a lumped port boundary condition (Fig. 4). The lumped port is treated as a lumped impedance rather than as a distributed network of elements and allows specifying input and output impedances at a specific location in the system.

After modeling the geometric environment, the FEA was performed by combining EM, fluidic, and thermal analysis. The time-harmonic EM analysis was used to numerically calculate the Joule heating based on global coil parameters (e.g., coil current I_0, frequency f_0). The total Joule heat is a combination of the self-heating of the coil and the eddy current heating of the Al frames. In addition, eddy currents in the coil due to self- and mutual inductance are considered as the EM field is resolved in the coil domain. The fluidic analysis includes temperature-dependent water cooling of the coil and the entire system using a simplified cooling module. A water flow velocity of $v = 0.66$ m/s with a temperature of $T_W = 20$ °C was specified in the boundary conditions. The thermal analysis was used to include the heat transfer mechanisms (Fig. 1) in the numerical calculation. The resulting inductive heating of the Al frames is illustrated in Fig. 5 for a VHF-industrial, scientific, and medical (VHF-ISM) radio band frequency of $f_0 = 40.68$ MHz, a current of $I_0 = 10$ A (amplitude), a coupling distance of $d = 0.5$ mm, and a heating time of $t_h = 10$ s. The FEA result shows a highly selective energy input to the Al frames with minor influence on the surrounding components. The average temperature of all frame geometries is $T_{\varnothing} = 626.5$ °C with a peak temperature of $T_{\max} = 641$ °C.

IV. INDUCTION HEATING BASED ON RADIO BAND FREQUENCIES

A. Experimental Setup

A key component of the experimental setup is the induction coil, which is based on the layout described in Fig. 3. The manufacturing was carried out in several process steps using surface and bulk micromachining. Fig. 6(a) shows the sections of the functional coil areas (fabrication, interconnection, and

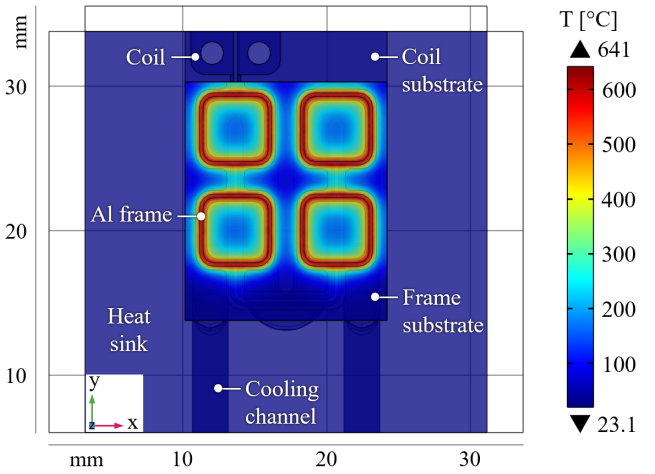

Fig. 5. FEA result of the volume temperature in the Al frames for $I_0 = 10$ A, $f_0 = 40.68$ MHz, and $t_h = 10$ s.

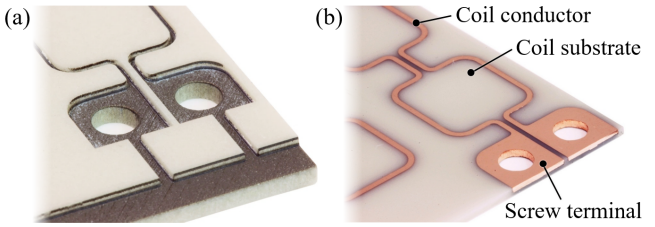

Fig. 6. Induction coil after fabrication. (a) Laser processing. (b) Cu ECD.

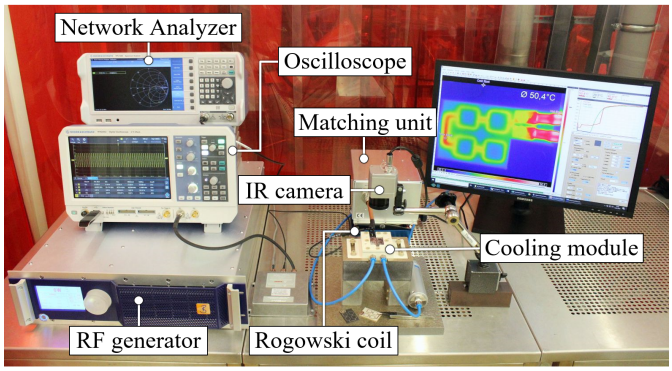

Fig. 7. Inductive heating setup with RF generator, automatic matching unit, water-cooled bonding module with integrated induction coil, and monitoring.

heating) produced by laser ablation. The finished coil after ECD, surface polishing, and dicing of the fabrication area is shown in Fig. 6(b).

Based on the FE simulation, the coil was integrated into a cooling module and electrically connected to the matching unit. The matching network automatically adapts the entire system to the standardized RF impedance of $Z_0 = 50\ \Omega$ to minimize losses due to reflected power during the process. The RF generator, delivering a maximum power of $P = 500$ W, served as the energy source for the inductive heating experiments. The in-line logging of the ac and frequency was carried out using a Rogwoski coil. An IR camera was used to determine the temperature distribution and heating rate in the process. The inductive heating setup is shown in Fig. 7.

B. Electrothermal Management

The inductive heating experiments were carried out at four frequencies in the HF and VHF range. A reference

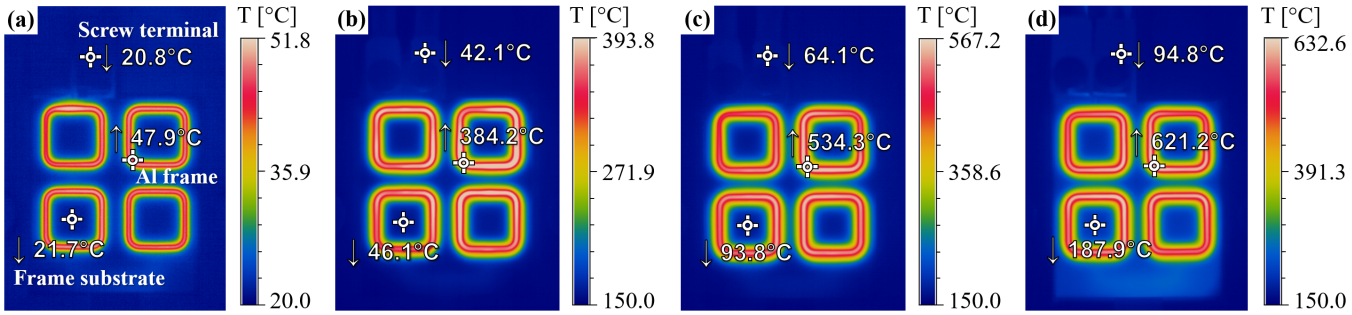

Fig. 8. IR images of the temperature distribution in the Al frames by induction heating with $t_h = 10$ s each. Heat map for (a) $I_{0-a} = 11.3$ A and $f_{0-a} = 1.94$ MHz, (b) $I_{0-b} = 10.7$ A and $f_{0-b} = 13.56$ MHz, (c) $I_{0-c} = 10.1$ A and $f_{0-c} = 27.12$ MHz, and (d) $I_{0-d} = 10.6$ A and $f_{0-d} = 40.68$ MHz.

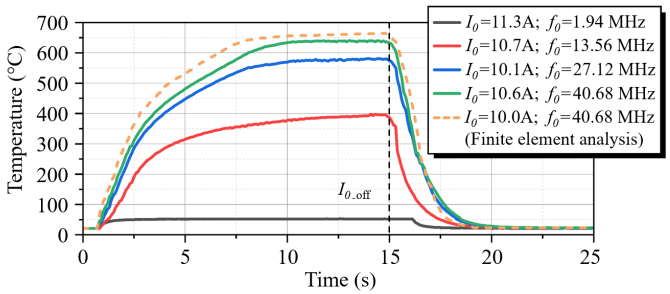

Fig. 9. Temperature–time curves of the inductively heated Al frames based on the experiments and a comparative FEA (dashed line).

frequency in the lower HF range, $f_{0-a} = 2$ MHz, was selected to demonstrate the efficiency of the frequency increase. To compare the results, the coil current was set to approximately $I_0 = 10$ A for each frequency. These currents correspond to an applied generator power of $P \leq 100$ W. Due to the frequency-dependent impedance matching and the resulting varying reflected power P_R, the current values are slightly different for each frequency. Related to (6) and the applied frequencies $f_{0-a} = 1.94$ MHz, $f_{0-b} = 13.56$ MHz, $f_{0-c} = 27.12$ MHz, and $f_{0-d} = 40.68$ MHz, the calculated skin depths for Al at $T_{\text{amb}} = 20$ °C are $\delta_a = 60.25$ μm, $\delta_b = 22.79$ μm, $\delta_c = 16.11$ μm, and $\delta_d = 13.16$ μm. Analogous to the FEA, the coupling distance was $d = 0.5$ mm.

The IR images in Fig. 8 demonstrate a continuous temperature increase of the Al frames with rising frequency and a significant elevation from 2–13.56 MHz (corresponding to skin depth). Analogous to the FEA (Fig. 5), the heat map for $f_{0-d} = 40.68$ MHz [Fig. 8(d)] shows a highly selective and homogeneous heating process. The maximum temperature was determined to be $T_{\text{max}} = 632.6$ °C after $t_h = 10$ s. Thus, the average heating rate is $dT/dt = 63.3$ K/s. Fig. 9 shows the maximum frame temperatures for each frequency and coil current as a temperature versus time curve. In addition, the result of the FEA from Fig. 5 is shown for comparison. The curves show a temperature rise with increasing frequency as well as a high heating rate up to $t_h = 5$ s. A temperature plateau is reached for each frequency after approximately $t_h = 10$ s. Thus, an equilibrium is established between the applied and dissipated heat energy. This heat dissipation is particularly noticeable after the coil current is switched off (I_{0_off}), resulting in the frame cooling to almost room temperature in $\Delta t = 5$ s.

V. Conclusion

An inductive heating process in the HF and VHF range was presented. By using the international ISM radio band frequencies, the process can be transferred and scaled to ISM applications without license issues. The technique allows rapid and selective heating of 2.0 μm thick Al layers close to its melting point with limited thermal impact on surrounding components (e.g., substrates, operational elements). Thus, induction heating combined with CMOS-compatible Al as a thin-film layer can serve as the basis for converting conventional Al–Al TCB into a liquid-phase process based on fusion welding. This offers exciting new opportunities in the field of MEMS packaging and heterogeneous integration. The upscaling of the technique to wafer level and its application to further heterogeneous bonding processes will be the subject of future work. In addition, further development in the field of impedance-controlled matching networks is required.

Acknowledgment

This work was supported in part by the German Federal Ministry of Economic Affairs and Energy (BMWi) and in part by the German Federation of Industrial Research Associations (AiF) within the Zentrales Innovationsprogramm Mittelstand (ZIM) Project "Ultra High Frequency (UHF)-Bond" [Förderkennzeichen (FK)] under Grant 16KN084039. The authors gratefully acknowledge the cooperation of their project partners barthel HF-Technik GmbH and Bach Resistor Ceramics GmbH.

References

[1] J. H. Lau, *Heterogeneous Integrations*, 1st ed. Singapore: Springer, 2019.

[2] M. Esashi, *3D and Circuit Integration of MEMS*, 1st ed. Weinheim, Germany: Wiley, 2021.

[3] P. Ramm, J.-Q. Lu, and M. V. Taklo, *Handbook of Wafer Bonding*, 1st ed. Weinheim, Germany: Wiley, 2012.

[4] A. W. Y. Tan and F. E. H. Tay, "Localized laser assisted eutectic bonding of quartz and silicon by Nd:YAG pulsed-laser," *Sens. Actuators A, Phys.*, vol. 120, no. 2, pp. 550–561, May 2005.

[5] J. Braeuer and T. Gessner, "A hermetic and room-temperature wafer bonding technique based on integrated reactive multilayer systems," *J. Micromech. Microeng.*, vol. 24, pp. 1–9, Oct. 2014.

[6] V. Rudnev, D. Loveless, and R. L. Cook, *Handbook of Induction Heating*, 2nd ed. Boca Raton, GL, USA: CRC Press, 2017.

[7] C. Hofmann et al., "Localized induction heating of Cu–Sn layers for rapid solid–liquid interdiffusion bonding based on miniaturized coils," *Micromachines*, vol. 13, no. 8, pp. 1–24, Aug. 2022.

[8] C. Hofmann et al., "Silver sintering technology based on induction heating for chip level bonding," in *Proc. IEEE CPMT Symp. Jpn.*, Nov. 2021, pp. 33–36.

[9] N. Malik, K. Schjølberg-Henriksen, E. U. Poppe, M. M. V. Taklo, and T. G. Finstad, "Impact of SiO_2 on Al–Al thermocompression wafer bonding," *J. Micromech. Microeng.*, vol. 25, no. 3, pp. 1–9, Feb. 2015.

[10] S. J. Doshi, A. V. Gohil, N. Mehta, and S. Vaghasiya, "Challenges in fusion welding of Al alloy for body in white," *Mater. Today, Proc.*, vol. 5, no. 2, pp. 6370–6375, 2018.